H$_2$O Maser Outflow from the Red Supergiant Star NML Cygni Observed with Japanese VLBI Network

Takumi NAGAYAMA,[1] Koji TAKEDA,[1] Toshihiro OMODAKA,[2] Hiroshi IMAI,[2] Seiji KAMENO,[2] Yoshiaki SOFUE,[2]
Akihiro DOI,[3] Kenta FUJISAWA,[4] Asao HABE,[5] Mareki HONMA,[6,7] Noriyuki KAWAGUCHI,[6,7] Eiji KAWAI,[8]
Hideyuki KOBAYASHI,[6,9] Yasuhiro KOYAMA,[8] Yasuhiro MURATA,[3,10] Kazuo SORAI,[5] Hiroshi SUDOU,[11]
Hiroshi TAKABA,[11] Sayaka TAMURA,[2,10] and Ken-ichi WAKAMATSU[11]

[1]*Graduate School of Science and Engineering, Kagoshima University, 1-21-35 Korimoto, Kagoshima, kagoshima 890-0065*
nagayama@astro.sci.kagoshima-u.ac.jp
[2]*Faculty of Science, Kagoshima University, 1-21-35 Korimoto, Kagoshima, kagoshima 890-0065*
[3]*Institute of Space and Astronautical Science, Japan Aerospace Exploration Agency,*
3-1-1 Yoshinodai, Sagamihara, Kanagawa 229-8510
[4]*Faculty of Science, Yamaguchi University, 1677-1 Yoshida, Yamaguchi, Yamaguchi 753-8512*
[5]*Department of Physics, Faculty of Science, Hokkaido University, N10W8, Sapporo 060-0810*
[6]*National Astronomical Observatry of Japan, 2-21-1 Osawa, Mitaka, Tokyo 181-8588*
[7]*Department of Astronomical Science, The Graduate University for Advanced Studies (SOKENDAI),*
2-21-1 Osawa, Mitaka, Tokyo 181-8588
[8]*Kashima Space Research Center, National Institute of Information and Communications Technology,*
893-1 Hirai, Kashima, Ibaraki 314-8510
[9]*Mizusawa VERA Observatory, 2-12 Hoshigaoka, Mizusawa, Oshu, Iwate 023-0861*
[10]*Department of Space and Astronautical Science, The Graduate University for Advanced Studies (SOKENDAI),*
3-1-1 Yoshinodai, Sagamihara, Kanagawa 229-8501
[11]*Faculty of Engineering, Gifu University, 1-1 Yanagido, Gifu, Gifu 501-1193*

Abstract

We present the proper motions of H$_2$O masers in NML Cygni, observed with the Japanese VLBI Network at three epochs spanning 455 d. We detected about 15 maser features at each epoch. Overall, 13 features that were detected at least twice were tracked by their radial velocities and proper motions. The three-dimensional kinematics of the maser features indicate the presence of an expanding outflow. The major axis of the outflow is estimated to be at a position angle of $\sim 108°$, and an inclination angle of $\sim 8°$ with respect to the line of sight. The H$_2$O masers are located between an apparent minimum radius of $\sim 9.6 \times 10^{12}$ m (64 AU) and a maximum radius of $\sim 3.0 \times 10^{13}$ m (202 AU), where the expansion velocity increases from 12 to 27 km s^{-1}. A comparison with the distributions of SiO, H$_2$O, and OH masers suggests that the outflow of NML Cygni is expanding outside a radius of $\sim 1.5 \times 10^{13}$ m (100 AU). This radius corresponds to 6 stellar radii, and is consistent with the radius of the inner boundary for the dust shell.

Key words: masers — stars: individual (NML Cygni) — stars: kinematics — stars: supergiants

1. Introduction

NML Cygni (hereafter NML Cyg) is a red supergiant that has an estimated mass of 50 $M_\odot$ and a luminosity of $5 \times 10^5 L_\odot$ at a distance of ~ 2 kpc (Morris & Jura 1983). This implies that NML Cyg is an important object in the sense that it may be a unique star in the latest stage of evolution, which is massive enough to become a supernova. We may be observing the envelope of a supernova precursor in great detail.

Very long baseline interferometry (VLBI) monitoring observations of H$_2$O masers provide a unique tool for studying the structures and kinematics of evolved stars. Analyses of the spatial positions, Doppler velocities, and proper motions of H$_2$O masers have revealed the three-dimensional gas kinematics of circumstellar envelopes (CSEs) (e.g., Marvel 1996).

In NML Cyg, the SiO, H$_2$O, and OH masers are detected at increasing velocities and angular separations from the star. The maximum expansion velocity is 27 km s^{-1} in OH 1612 MHz (Etoka & Diamond 2004) and SiO masers are closest to the stellar velocity (v_*) of ~ 0 km s^{-1}. But unusually, at one epoch, Boboltz and Marvel (2000) observed a twin-peaked SiO spectrum, which led them to postulate that v_* is -6.6 ± 0.1 km s^{-1} and that the SiO masers were rotating. Observations of H$_2$O maser emission since 1969 show that it is dominated by a complex of blue-shifted peaks around -20 km s^{-1}, with fainter emission ranging over 40 km s^{-1}, including a secondary peak red-shifted with respect to $v_* \sim 0$ km s^{-1} (Schwartz & Barrett 1970; Richards et al. 1996). This is similar to the OH 1612 MHz profile, which also had a brighter blue-shifted peak for more than 3 decades (Masheder et al. 1974; Etoka & Diamond 2004).

Although $v_* = -6.6 \pm 0.1$ km s^{-1} was estimated by Boboltz and Marvel (2000), $v_* = 0 \pm 2$ km s^{-1} was suggested by almost all other observations in molecular lines and masers (Kemper

et al. 2003; Etoka & Diamond 2004; reviewed in Richards et al. 1996). In the present paper, we adopt $v_* = 0 \pm 2\,\mathrm{km\,s^{-1}}$.

It is suggested that NML Cyg has an asymmetric CSE based on the OH 1612 MHz and H_2O masers (Diamond et al. 1984; Richards et al. 1996). In order to investigate the kinematics of the outflow, which may be related to this asymmetry, we measured the proper motions of 22.2 GHz H_2O masers. Section 2 describes the observations with the Japanese VLBI Network (JVN) and data reduction. Section 3 shows the distribution and proper motions of H_2O masers. Section 4 discusses the kinematics of the expanding outflow of NML Cyg through a comparison with previous observations. Although the distance to NML Cyg is uncertain, most authors have favored that NML Cyg is indeed at the distance of the Cyg OB2 association, 2 kpc (e.g., Morris & Jura 1983; Richards et al. 1996). We therefore adopt the distance of 2 kpc to this source.

2. Observations

VLBI observations were made on 2006 January 30, 2007 January 29, and 2007 April 30, using four or six telescopes of the JVN, which consists of four 20-m telescopes of the VLBI Exploration of Radio Astrometry (VERA) of the National Astronourical Observatory of Japan (NAOJ), a 34-m telescope of the National Institute of Information and Communications Technology (NICT) at Kashima, and an 11-m telescope of Hokkaido University at Tomakomai. The status of the telescopes, data reduction, and resulting performances in the individual epoch are summarized in table 1. Although VERA with a dual-beam system is dedicated to phase-referencing observations (Kobayashi et al. 2003), we made single-beam VLBI observations, because the phase reference source for NML Cyg was not found. NML Cyg and calibrators (ICRF J203837.0+511912 and ICRF J202510.8+334300) were observed for 10 hr and 8 hr in the first and later epochs, respectively. Left-hand circular-polarization signals at 22 GHz were acquired in a digital form with the able K-4 (Kiuchi et al. 1997) and the VSOP terminals (Iguchi et al. 2000) with a data rate of 128 Mbps, and in two base band channels with a band width of 16 MHz each, covering a radial velocity span of 215.7 $\mathrm{km\,s^{-1}}$. The correlation was carried out with the Mitaka FX correlator (Shibata et al. 1998). The correlation outputs consisted of 1024 velocity channels, yielding a frequency and a velocity spacing of 15.625 kHz

and $0.21\,\mathrm{km\,s^{-1}}$, respectively. In the first epoch, the outputs consisted of 512 velocity channels, yielding a velocity spacing of $0.42\,\mathrm{km\,s^{-1}}$.

Amplitude and phase calibrations, fringe fitting, and imaging were performed using the Astronomical Image Processing System (AIPS) of the National Radio Astronomy Observatory (NRAO). Calibrations of the clock parameters, bandpass characteristics, visibility amplitudes, radial velocity, and phase fluctuation due to the atmosphere were carried out in the standard manner. The clock parameters (clock offset and clock rate offset) were calibrated using the residual delays and delay rates for the calibrator sources observed every hour. A bandpass calibration was also applied using a power spectrum derived from autocorrelation functions toward the calibrators. The amplitude calibration was made using the system noise temperatures; they were evaluated by the "R-Sky" method, by observing a reference black body at the beginning of each scan (typically every hour). The observed radio frequencies of the spectral channels were converted to the LSR velocities (v_{LSR}, radial velocities with respect to the local standard of rest) using a rest frequency of 22.235080 GHz. For phase calibrations, the visibilities of all velocity channels were phase referenced to those in the reference velocity channel with a maser spot at an LSR velocity of $5.6\,\mathrm{km\,s^{-1}}$, which is one of the brightest spots, and shows no sign of complicated structure according to the closure phase deviation from zero. A typical size of the synthesized beam was ~ 1 milliarcsecond (mas) through the three epochs.

We identified all emission components stronger than 7-times the rms noise level for each spectral channel. The position of the brightness peak in the detected components were estimated using the AIPS task SAD by assuming a two-dimensional Gaussian brightness distribution. We could see several spots that are clustered within a small region in space and Doppler velocity, typically 1 mas (2 AU) and 1 $\mathrm{km\,s^{-1}}$, respectively. We defined this cluster of spots as a feature. The feature position is defined as that of the brightness peak in the spots. The relative position uncertainties for the features were 0.03–0.24 mas. We detected 16, 13, and 14 maser features in the three epochs.

3. Results

3.1. Spectrum

Figure 1 shows the total power spectrum of H_2O masers in NML Cyg obtained with the VERA Mizusawa 20-m telescope

Table 1. Status of the telescopes, data reduction, and resulting performances in the individual epoch of the JVN observations.

Epoch	Date	Duration (hr)	Used telescopes*	1-σ level noise (Jy beam^{-1})	Synthesized beam[†] (mas)	Number of detected features
1 ...	2006 Jan 30	10	MZ, IR, OG, IS, KS, TM	0.040	$1.2 \times 1.0, -16°$	16
2 ...	2007 Jan 29	8	MZ, IR, IS, KS	0.052	$2.9 \times 0.9, -39°$	13
3 ...	2007 Apr 30	8	MZ, IR, OG, IS, KS, TM	0.039	$1.6 \times 1.1, -75°$	14

* Telescopes that were effectively operated and whose recorded data were valid: MZ: the VERA 20-m telescope at Mizusawa, IR: the VERA 20-m telescope at Iriki, OG: the VERA 20-m telescope at Ogasawara, IS: the VERA 20-m telescope at Ishigakijima, KS: the NICT 34-m telescope at Kashima, TM: the Hokkaido University 11-m telescope at Tomakomai.

[†] The synthesized beam made in natural weighted visibilities; major and minor axis lengths and a position angle.
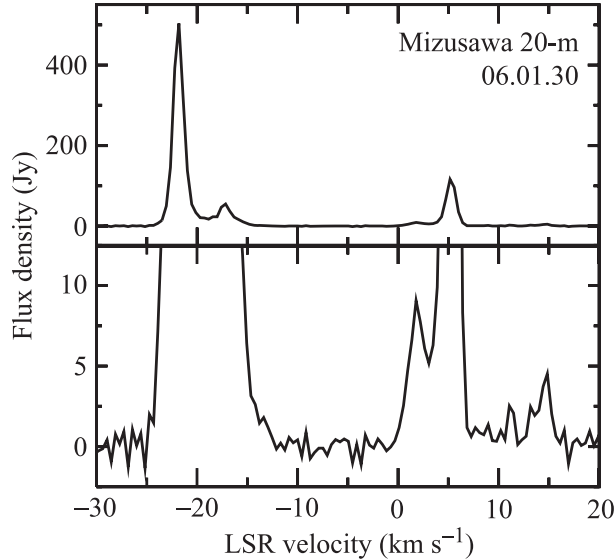
Fig. 1. H₂O maser spectrum in NML Cyg obtained with the Mizusawa 20-m telescope.

Fig. 2. Distributions and proper-motion vectors of H₂O masers in NML Cyg. The color index denotes the LSR velocity range from -22.2 to $15.5\,\mathrm{km\,s^{-1}}$, where 22 features are located. The map origin is located at the position of the reference maser feature at $v_{\mathrm{LSR}} = 5.6\,\mathrm{km\,s^{-1}}$, which is estimated to be α(J2000)= $20^{\mathrm{h}}46^{\mathrm{m}}25\overset{\mathrm{s}}{.}543 \pm 0\overset{\mathrm{s}}{.}008$ and δ(J2000)= $40°06'59\overset{''}{.}42 \pm 0\overset{''}{.}10$ from a fringe rate analysis. The displayed proper-motion vector is that subtraced by a velocity bias, $(\mu_x, \mu_y) = (0.19, -0.28)\,(\mathrm{mas\,yr^{-1}})$, from the original vector to cancel out the average motions of all features.

at the first epoch. The H₂O maser emission spreads in an LSR velocity range from -25 to $17\,\mathrm{km\,s^{-1}}$. We confirmed most of the velocity components detected in previous observations (Johnston et al. 1985; Yates et al. 1995; Richards 1997). The peak flux density of $\sim 450\,\mathrm{Jy}$ is one order of magnitude larger than that in the previous observations. The peak flux density was obtained at around $40\,\mathrm{Jy}$ in 1993 (Yates et al. 1995), and $60\,\mathrm{Jy}$ in 1996 (Richards 1997).

A Very Long Baseline Array (VLBA) observation showed that the H₂O maser emission of NML Cyg is significantly resolved out (Marvel 1996). The correlated flux obtained with the Kashima–Mizusawa baseline (length of $355\,\mathrm{km}$), which is the most sensitive and has the second-shortest baseline in our observation, was $\sim 30\%$ of the total power flux.

The brightest and most blueshifted component ($v_{\mathrm{LSR}} = -21.8\,\mathrm{km\,s^{-1}}$) appears to exhibit a velocity drift. The LSR velocities of this component in 1981, 1993, and 2006 were -18, -20, and $-21.8\,\mathrm{km\,s^{-1}}$, respectively. These values were shifted with respect to $v_* = 0 \pm 2\,\mathrm{km\,s^{-1}}$. The derived acceleration was $\dot{v} = -0.2$ to $-0.1\,\mathrm{km\,s^{-1}\,yr^{-1}}$ in the line of sight. The acceleration of $|\dot{v}| = 0.09–0.26\,\mathrm{km\,s^{-1}\,yr^{-1}}$ was also measured at five components ($v_{\mathrm{LSR}} = -21.4$, -17.9, -16.7, 2.4, and $5.6\,\mathrm{km\,s^{-1}}$) by single-dish monitoring observations (Shintani et al. 2008). Our derived acceleration was consistent with that of Shintani et al. (2008).

3.2. Distribution

Figure 2 shows the distributions and proper motion vectors of H₂O maser feautes in NML Cyg (for proper motions, see next subsection). Twenty-two features detected during at least one epoch are plotted. These features are distributed within a region of $130\,\mathrm{mas} \times 150\,\mathrm{mas}$ ($260\,\mathrm{AU} \times 300\,\mathrm{AU}$). This region size is approximately $1/1.5$ of that obtained with the previous MERLIN observation (Richards et al. 1996). This might be affected by missing flux and resolving out. As mentioned above, the H₂O maser emission was resolved out in JVN
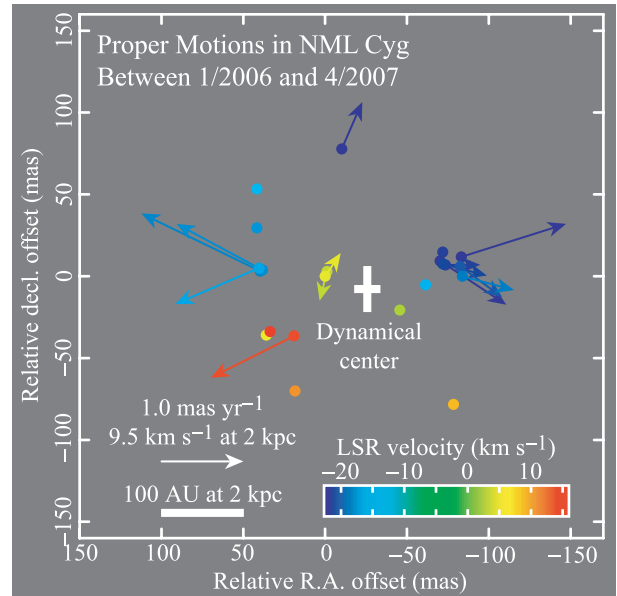
observations with an $\sim 1\,\mathrm{mas}$ beam, while the MERLIN observation with an $\sim 13\,\mathrm{mas}$ beam detected almost all of the total power flux. The blueshifted ($v_{\mathrm{LSR}} = -22.2$ to $-12.5\,\mathrm{km\,s^{-1}}$) and redshifted ($v_{\mathrm{LSR}} = 3.0$ to $15.5\,\mathrm{km\,s^{-1}}$) features were distributed in the north and south, respectively. This velocity distribution was consistent with that of MERLIN.

The MERLIN image shows a pair of outlying features to the northwest (NW) and southeast (SE) (position angel $\approx 132°$) separated by $\sim 600\,\mathrm{mas}$. However, our JVN observations could not detect these features. This wolud be because the intensity of the SE feature was weak and the NW and SE features were resolved out. The SE feature with $v_{\mathrm{LSR}} = -5.3$ to $-3.2\,\mathrm{km\,s^{-1}}$ was not detected, even by the total power spectrum. Since the NW feature is greatly extended with respect to an $\sim 1\,\mathrm{mas}$ beam, it may be resolved out by VLBI observations. The size of the NW feature ($27\,\mathrm{mas}$) is three-times larger than the typical feature size ($8\,\mathrm{mas}$) of NML Cyg (Richards et al. 1996). The SE and NW features were not detected even by VLBA observations, which were made in the same year as the MERLIN observation (Marvel 1996).

3.3. Proper Motions

Table 2 lists the observed positions and the proper motions of 22 maser features in NML Cyg. We considered the maser features in different epochs as being the *same* features, if their LSR velocities were equal to each other within $0.42\,\mathrm{km\,s^{-1}}$, and if their positions were coincident within the angular separation that corresponds to a proper motion of $50\,\mathrm{km\,s^{-1}}$ ($5.3\,\mathrm{mas\,yr^{-1}}$). Based on these criteria, 13 maser features

Table 2. Positions and proper motions of the H$_2$O maser features in NML Cyg.

ID[*]	LSR velocity (km s^{-1})	Offset[†] (mas)				Proper motion[†] (mas yr^{-1})				Epochs[‡]
	v_{LSR}	X	σX	Y	σY	μ_x	$\sigma\mu_x$	μ_y	$\sigma\mu_y$	
1	−22.22	−83.18	0.24	11.86	0.16	−1.09	0.10	0.12	0.08	101
2	−22.22	−70.25	0.16	9.37	0.05	−0.62	0.09	−0.82	0.08	101
3	−22.22	−10.11	0.10	77.71	0.08	−0.06	0.17	0.29	0.11	110
4	−21.80	−73.58	0.10	6.87	0.08	−0.23	0.14	−0.28	0.10	111
5	−21.37	−71.85	0.18	14.70	0.10	—	—	—	—	001
6	−20.95	−71.95	0.06	7.55	0.04	−0.35	0.16	−0.43	0.04	111
7	−20.11	−82.58	0.14	6.02	0.14	−0.32	0.09	−0.66	0.12	101
8	−18.00	−83.84	0.10	−0.10	0.10	−0.44	0.21	−0.45	0.05	111
9	−17.58	39.67	0.08	3.17	0.08	1.64	0.09	0.42	0.11	110
10	−17.38	38.23	0.22	3.78	0.22	1.24	0.51	0.28	0.45	011
11	−16.95	41.59	0.17	29.47	0.10	—	—	—	—	001
12	−16.32	40.42	0.20	5.05	0.14	1.22	0.13	−0.73	0.12	111
13	−14.85	−61.40	0.17	−5.32	0.24	—	—	—	—	010
14	−12.53	41.76	0.16	53.36	0.12	—	—	—	—	100
15	3.05	−45.69	0.05	−20.73	0.11	—	—	—	—	001
16	3.90	−1.10	0.16	2.84	0.10	0.28	0.12	−0.64	0.10	111
17	5.58	0.00	0.03	0.00	0.03	0.00	0.03	0.00	0.03	111
18	6.00	35.97	0.18	−35.90	0.18	—	—	—	—	100
19	9.79	−78.43	0.14	−78.31	0.07	—	—	—	—	100
20	11.90	18.36	0.19	−70.08	0.14	—	—	—	—	010
21	14.85	19.05	0.08	−36.53	0.06	1.21	0.18	−0.79	0.07	111
22	15.48	33.58	0.16	−33.87	0.18	—	—	—	—	010

[*] Feature ID number.
[†] Relative value with respect to the position-reference maser feature: ID 17.
[‡] Detected epochs: "1" for detection, and "0" for non-detection.

were identified in at least two epochs. The proper motions were calculated by performing a linear least-squares fit to the position offsets against the elapsed time. Figure 3 shows the observed time variations of the right ascension (RA) and declination (Dec) offsets (relative to ID 17).

The proper motions exhibit an expanding outflow structure. To obtain the dynamical center of the outflow, we take a simplest model, assuming that the maser features were projected with the calculated proper motions from a single origin at the same time. The basic method is shown in Imai et al. (2000). The dynamical center was calculated by performing a linear least-squares fit to the positions of features against the obtained proper motions. The center is located at $(X,\ Y) = (-26 \pm 8,\ -8 \pm 14)$ (mas) which is indicated by a cross symbol in figure 2.

We obtained the mean velocities and the velocity dispersions along the x, y, and z axes to be $(|\bar{v}_x|,\ |\bar{v}_y|,\ |\bar{v}_z|) = (6.8, 3.8, 17.1)$ (km s^{-1}), and $(\sigma_{vx}, \sigma_{vy}, \sigma_{vz}) = (7.8, 4.1, 18.1)$ (km s^{-1}), respectively. The mean velocity and velocity dispersion along the z-axis are the largest.

4. Discussion

4.1. Major Axis of Outflow Estimated Based on an Analysis with VVCM

To obtain the axis of the outflow, we made an analysis based on the velocity variance–covariance matrix (VVCM)

of the maser velocity vectors (Bloemhof 2000). The VVCM diagonalization provides eigenvectors and eigenvalues for the VVCM; the eigenvector corresponding to the largest eigenvalue indicates the kinematical axis of the outflow, and the eigenvalue gives a velocity dispersion along the axis. The VVCM consists of elements calculated from the velocity dispersions, as follows (units of km^2 s^{-2}):

$$\sigma_{ij} = \frac{1}{N-1}\sum_{n=1}^{N}(v_{i,n} - \bar{v}_i)(v_{j,n} - \bar{v}_j), \tag{1}$$

where i and j denote three orthogonal space axes (e.g., RA, Dec, and radial coordinate z), and n is the n-th maser motion in a collection totaling N. We used the average velocity in the z-axis of $\bar{v}_z = v_* = 0 \pm 2$ km s^{-1}. The diagonalized VVCM was obtained as follows:

$$A = \begin{pmatrix} \sigma_{xx} & \sigma_{yx} & \sigma_{zx} \\ \sigma_{xy} & \sigma_{yy} & \sigma_{zy} \\ \sigma_{xz} & \sigma_{yz} & \sigma_{zz} \end{pmatrix}$$

$$= \begin{pmatrix} 66.18 & 5.26 & 37.83 \\ 5.26 & 18.31 & -14.74 \\ 37.83 & -14.74 & 354.28 \end{pmatrix}, \tag{2}$$

$$P = \begin{pmatrix} -0.1505 & 0.9804 & 0.1270 \\ 0.9868 & 0.1567 & -0.0408 \\ 0.0599 & -0.1192 & 0.9911 \end{pmatrix}, \tag{3}$$
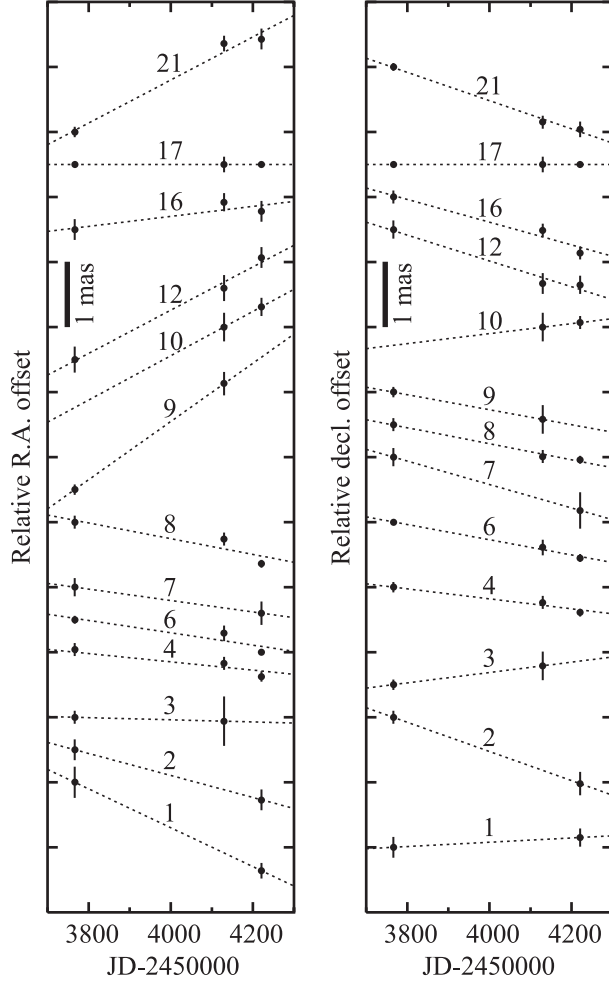
Fig. 3. Observed relative proper motions of the H₂O maser features in NML Cyg. A number added for each maser feature shows the assigned one listed in table 2. A dash line indicates a least-squares-fitted line, assuming a constant velocity motion of the maser feature.

$$P^{-1}AP = \begin{pmatrix} 16.61 & 0 & 0 \\ 0 & 62.42 & 0 \\ 0 & 0 & 359.73 \end{pmatrix}. \tag{4}$$

In equation (4), one eigenvalue is large compared with another. This would imply a bipolarity of the outflow. The eigenvector corresponding to the largest eigenvalue (velocity dispersion) had a position angle of $108 \pm 4°$ and an inclination angle of $8 \pm 3°$ with respect to the line of sight. The uncertainties of the obtained values were estimated by a Monte-Carlo simulation, generating VVCMs with artificial errors around the values obtained in the measurement. The obtained position angle almost agrees with the elongation of OH masers (Masheder et al. 1974).

4.2. Environment of the Circumstellar Envelope

To estimate the spatial locations and expansion velocities of individual maser features in the outflow, we adopted an expanding shell model; the shell consists of a series of thin shells, each of which satisfies the equation for the observed radial velocity and the projected distance from the star (v, r)
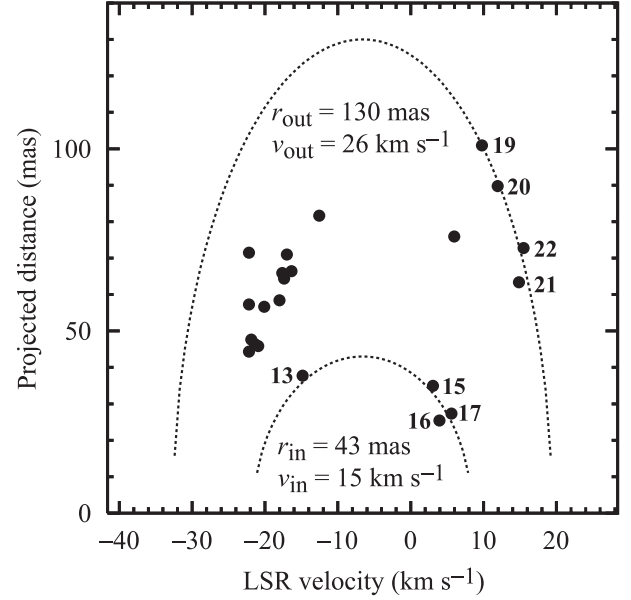

Fig. 4. Projected distance–LSR velocity diagram of the H₂O maser features in NML Cyg. The modeled inner and outer boundaries of shell are indicated by dashed lines.

as

$$\left(\frac{r}{r_{\text{shell}}}\right)^2 + \left(\frac{v - v_{\text{sys}}}{v_{\text{exp}}}\right)^2 = 1. \tag{5}$$

Here, r_{shell} is the radius of the thin shell, v_{exp} the expansion velocity of the thin shell, and v_{sys} the systemic velocity of NML Cyg. Figure 4 shows the projected distance–LSR velocity diagram of the maser features. We used a systemic velocity of $v_{\text{sys}} = v_* = 0 \pm 2\,\text{km s}^{-1}$. Least-squares fits using equation (5) to the data of three maser features (ID 15, 16, and 17 in table 2 and figure 4) give an inner radius of $r_{\text{in}} = 32 \pm 7\,\text{mas}$ ($64 \pm 14\,\text{AU}$), and an expansion velocity of $v_{\text{in}} = 12 \pm 5\,\text{km s}^{-1}$. Using the data of ID 1, 2, 3, 19 and 22, an outer radius and an expansion velocity were obtained to be $r_{\text{out}} = 101 \pm 12\,\text{mas}$ ($202 \pm 24\,\text{AU}$) and $v_{\text{out}} = 27 \pm 3\,\text{km s}^{-1}$, respectively. The radius of the central star was obtained to be $R_* = 8.1\,\text{mas}$ ($16.2\,\text{AU}$) from a $2.13\,\mu\text{m}$ observation with the 6-m telescope at the Special Astrophysical Observatory (Blöcker et al. 2001). The H₂O masers are distributed within a range of 4–$13\,R_*$.

The increase in the expansion velocity with distance from the star is parameterized by the logarithmic velocity gradient, $\epsilon = d(\ln v)/d(\ln r)$ (Richards et al. 1996). The logarithmic velocity gradient of NML Cyg was derived to be $\epsilon = 0.70^{+1.05}_{-0.47}$. This value is almost consistent with $\epsilon = 0.30$, which was derived in the MERLIN observation (Richards et al. 1996). The value is similar to those found in the other supergiants ($\epsilon = 0.50$–1.20, S Per, VY CMa, and VX Sgr) and slightly lower than the semi-regular and Mira variables ($\epsilon = 0.78$–3.50, R Crt, RT Vir, and IK Tau) (Ishitsuka et al. 2001, see also references therein). Thus, the velocity gradient is relatively flat in the CSEs in supergiants compared with those in semi-regular and Mira variables.

4.3. Comparison with SiO, H_2O, and OH Masers, and Dust

The masers of CSE in NML Cyg are distributed with actual radii of ~ 50 mas for $v = 0$, $J = 1$–0 SiO (Boboltz & Claussen 2004), ~ 70 mas for H_2O, and $\sim 1''$ for OH masers (Etoka & Diamond 2004). The blueshifted and redshifted features of these masers lie to the north (west), and south (east), respectively. The expansion velocities are $\leq 18\,\mathrm{km\,s^{-1}}$ for SiO (Boboltz & Claussen 2004), 12–27 $\mathrm{km\,s^{-1}}$ for H_2O, and 16–27 $\mathrm{km\,s^{-1}}$ for OH (Etoka & Diamond 2004). The expansion velocity of the SiO maser was estimated from half of the velocity range of the spectrum. At a radius of $\gtrsim 50$ mas (100 AU), the expansion velocity of the outflow seems to increase with the distance from the star.

The more compact distribution within a radius of ~ 30 mas (60 AU) is traced by the $v = 1$, $J = 1$–0 SiO maser. Boboltz and Marvel (2000) showed that the blueshifted and redshifted features of this maser lie to the southwest, and northeast, respectively, and suggested that this maser is associated with the rotating ring. The velocity distribution of this maser is different from those of the $v = 0$, $J = 1$–0 SiO, H_2O, and OH masers. Therefore, the outflow of NML Cyg appears to be expanding outside a radius of 50 mas (100 AU). This radius is consistent with that of the inner boundary for the dust shell at $2.13\,\mu\mathrm{m}$ (52.5 mas: Blöcker et al. 2001). We suggest that the outflow with increasing velocity would be expanding from the inner boundary of the dust shell.

4.4. Mass-Loss Rate

We estimated the mass-loss rate using a method of Richards, Yates, and Cohen (1998). The mass-loss rate is given by $\dot{M} = 4\pi r_{\mathrm{in}}^2 v_{\mathrm{in}} \rho_{\mathrm{q}}$, where ρ_{q} is the quenching density with the assumption that the mean particle mass is 1.37-times the mass of molecular hydrogen. We assumed a number density in the masing region of $n(H_2) \sim 10^{15}\,\mathrm{m^{-3}}$ (Elitzur 1992; Yates et al. 1997). Taking an inner radius of $r_{\mathrm{in}} \sim 64\,\mathrm{AU}$, and an expansion velocity of $v_{\mathrm{in}} \sim 12\,\mathrm{km\,s^{-1}}$, we could estimate the mass-loss rate to be $\dot{M} \sim 10^{-3}\,M_\odot\,\mathrm{yr^{-1}}$.

This mass-loss rate is one order of magnitude larger than the value, $\dot{M} = (1.6\text{–}1.8) \times 10^{-4}\,M_\odot\,\mathrm{yr^{-1}}$, derived from the CO and SiO thermal emissions (Knapp et al. 1982; Lucas et al. 1992). The result, in which the mass-loss rate calculated from H_2O masers is larger than those estimated from the molecular lines is also found in VY CMa (Richards et al. 1998), S Per (Richards et al. 1999), VX Sgr (Murakawa et al. 2003), and the AGB stars (Bains et al. 2003). This is because there would be an irregularity of the density in the CSE, and the H_2O masers would occur in discrete patches of higher density than the wind average at the same distance from the star.

5. Conclusions

We carried out three epoch observations of H_2O masers in NML Cyg with JVN, and successfully measured their proper motions. The following conclusions are drawn from the present study:

1. From an analysis based on a VVCM of H_2O maser motions, the kinematical axis of the outflow is estimated to have a position angle of $\sim 108°$ and an inclination angle of $\sim 8°$.
2. The H_2O masers are associated with outflow with inner and outer radii of ~ 32 mas (64 AU), and ~ 101 mas (202 AU), respectively, and an expansion velocity of $\sim 12\,\mathrm{km\,s^{-1}}$ while increasing to $\sim 27\,\mathrm{km\,s^{-1}}$.
3. We derived the mass-loss rate of NML Cyg to be $\dot{M} \sim 10^{-3}\,M_\odot\,\mathrm{yr^{-1}}$ from the inner radius and expansion velocity. This mass-loss rate is one order of magnitude larger than those measured by the CO and SiO thermal emissions. This larger value may be related to the fact that H_2O masers occur in discrete patches of higher density than the wind average at the same distance from the star.
4. A comparison with the spatial- and velocity- distributions of $v = 1$, $J = 1$–0 SiO (Boboltz & Marvel 2000), $v = 0$, $J = 1$–0 SiO (Boboltz & Claussen 2004), H_2O, and OH (Etoka & Diamond 2004) masers suggests that the outflow in NML Cyg is expanding outside a radius of ~ 50 mas (100 AU). The radius of ~ 50 mas is consistent with the radius of the inner boundary for the dust shell.

References

Bains, I., Cohen, R. J., Louridas, A., Richards, A. M. S., Rosa-González, D., & Yates, J. A. 2003, MNRAS, 342, 8

Blöcker, T., Balega, Y., Hofmann, K.-H., & Weigelt, G. 2001, A&A, 369, 142

Bloemhof, E. E. 2000, ApJ, 533, 893

Boboltz, D. A., & Claussen, M. J. 2004, ApJ, 608, 480

Boboltz, D. A., & Marvel, K. B. 2000, ApJ, 545, L149

Diamond, P. J., Norris, R. P., & Booth, R. S. 1984, MNRAS, 207, 611

Elitzur, M. 1992, Astronomical Masers (Dordrecht: Kluwer)

Etoka, S., & Diamond, P. 2004, MNRAS, 348, 34

Iguchi, S., Kawaguchi, N., Kameno, S., Kobayashi, H., & Kiuch, H. 2000, IEICE transactions on communications, 83, 406

Imai, H., Kameya, O., Sasao, T., Miyoshi, M., Deguchi, S., Horiuchi, S., & Asaki, Y. 2000, ApJ, 538, 751

Ishitsuka, J. K., et al. 2001, PASJ, 53, 1231

Johnston, K. J., Spencer, J. H., & Bowers, P. F. 1985, ApJ, 290, 660

Kemper, F., Stark, R., Justtanont, K., de Koter, A., Tielens, A. G. G. M., Waters, L. B. F. M., Cami, J., & Dijkstra, C. 2003, A&A, 407, 609

Kiuchi, H., Amagai, J., Hama, S., & Imae, M. 1997, PASJ, 49, 699

Knapp, G. R., Phillips, T. G., Leighton, R. B., Lo, K. Y., Wannier, P. G., Wootten, H. A., & Huggins, P. J. 1982, ApJ, 252, 616

Kobayashi, H., et al. 2003, ASP Conf. Ser., 306, 367

Lucas, R., et al. 1992, A&A, 262, 491

Marvel, K. B. 1996, Ph.D. Thesis, New Mexico State Univ.

Masheder, M. R. W., Booth, R. S., & Davies, R. D. 1974, MNRAS, 166, 561

Morris, M., & Jura, M. 1983, ApJ, 267, 179

Murakawa, K., Yates, J. A., Richards, A. M. S., & Cohen, R. J. 2003, MNRAS, 344, 1

Richards, A. M. S. 1997, Ph.D. Thesis, University of Manchester

Richards, A. M. S., Yates, J. A., & Cohen, R. J. 1996, MNRAS, 282, 665

Richards, A. M. S., Yates, J. A., & Cohen, R. J. 1998, MNRAS, 299, 319

Richards, A. M. S., Yates, J. A., & Cohen, R. J. 1999, MNRAS, 306, 954

Schwartz, P. R., & Barrett, A. H. 1970, ApJ, 159, L123

Shibata, K. M., Kameno, S., Inoue, M., & Kobayashi, H. 1998, in ASP Conf. Ser. 144, IAU Colloq. 164, Radio Emission from Galactic and Extragalactic Compact Sources, ed. J. A. Zensus, G. B. Taylor, & J. M. Wrobel (San Francisco: ASP), 413

Shintani, M., et al. 2008, PASJ, 60, 1077

Yates, J. A., Cohen, R. J., & Hills, R. E. 1995, MNRAS, 273, 529

Yates, J. A., Field, D., & Gray, M. D. 1997, MNRAS, 285, 303